JOURNAL OF THERMOPHYSICS AND HEAT TRANSFER
Vol. 23, No. 1, January–March 2009

Numerical Analysis of Heat Storage Phenomenon in a Dual Latent Heat Sink

Krishna M. Kota,* Louis C. Chow,† Jianhua Du,‡ and Jayanta S. Kapat§
University of Central Florida, Orlando, Florida 32816-2450
Quinn H. Leland¶
U.S. Air Force Research Laboratory, Wright–Patterson Air Force Base, Ohio 45433
and
Richard J. Harris**
University of Dayton Research Institute, Dayton, Ohio 45469

DOI: 10.2514/1.36386

This paper focuses on the numerical analysis of the heat storage phenomenon in a dual latent heat sink intended for low thermal duty cycle electronic heat sink applications. The effectiveness of this heat sink depends on the rapidness of the charging facility in the design during the pulse heat generation period of the duty cycle. Heat storage in this heat sink involves the transient simultaneous laminar film condensation of vapor and melting of an encapsulated phase change material in graphite foam. The key focus of this paper is to numerically analyze this conjugate heat transfer problem including the wall inertia effect and thus verify the effectiveness of the heat storage mechanism of the heat sink. An effective heat capacity formulation is employed for modeling the phase change problem and is solved using the finite element method. The results of the developed model showed that the concept is effective in preventing an undue temperature rise of the system.

Nomenclature

A = surface area of foam, m^2
a = specific surface area of the porous medium, m^2/m^3
Bi = Biot number
c_p = effective specific heat of the phase change material and foam composite, $J/kg \cdot K$
c_{pf} = specific heat of foam, $J/kg \cdot K$
c_{pl} = specific heat of the liquid phase of phase change material, $J/kg \cdot K$
c_{pm} = latent heat of fusion of phase change material averaged over the melting range, $J/kg \cdot K$
c_{ps} = specific heat of the solid phase of phase change material, $J/kg \cdot K$
c_{pw} = specific heat of the thermal energy storage unit column wall, $J/kg \cdot K$
d_p = pore diameter, μm
h = convection heat transfer coefficient, $W/m^2 \cdot K$
h_{int} = foam ligament and phase change material interfacial heat transfer coefficient, $W/m^2 \cdot K$
h_{lv} = latent heat of vaporization of the condensate, J/kg
h_{sf} = latent heat of fusion of the phase change material, J/kg
h_{sfo} = latent heat of fusion of the phase change material in the operating temperature range, J/kg
Ja = Jakob number
k = effective thermal conductivity tensor for the phase change material and foam composite, $W/m \cdot K$
k_c = thermal conductivity of condensate, $W/m \cdot K$
k_{fe} = effective out-of-plane thermal conductivity of foam ligaments, $W/m \cdot K$
k_{fy} = foam thermal conductivity in the Y direction, $W/m \cdot K$
k_{fz} = foam thermal conductivity in the Z direction, $W/m \cdot K$
k_l = thermal conductivity of the liquid phase of phase change material, $W/m \cdot K$
k_{PCM} = typical thermal conductivity of phase change material, $W/m \cdot K$
k_s = thermal conductivity of the solid phase of phase change material, $W/m \cdot K$
k_w = thermal conductivity of the thermal energy storage unit column wall, $W/m \cdot K$
k_{yy} = effective thermal conductivity of phase change material and foam composite in the Y direction, $W/m \cdot K$
k_{zz} = effective thermal conductivity of phase change material and foam composite in the Z direction, $W/m \cdot K$
L = height of phase change material and foam composite, m
N = number of fins per unit inch
Nu_p = pore Nusselt number
$\hat{n}$ = unit normal
Pr = Prandtl number
P_{sat} = vapor saturation pressure, K
$\mathbf{q}$ = heat flux, W/m^2
T = temperature field in phase change material and foam composite, K
T_{inf} = ambient temperature, K
T_m = melting temperature of the phase change material, K
T_v = vapor temperature, K
T_w = temperature field in column wall, K
T_{wall} = column outside wall temperature as governed by the conjugate problem, K
T_0 = initial temperature of the transient problem, K
t = temporal variable, s
time = temporal variable at which a numerical solution is stored, s
t_w = thickness of the solid walls of the column, m
V = volume of foam, m^3
W = width of the foam-filled phase change material composite, m
x = spatial coordinate in the Cartesian X direction, m
y = spatial coordinate in the Cartesian Y direction, m

Presented as Paper 1194 at the 46th AIAA Aerospace Sciences Meeting and Exhibit, Reno, Nevada, 7–10 January 2008; received 28 December 2007; revision received 29 August 2008; accepted for publication 8 September 2008.

*Student. Member AIAA.
†Professor and University Chair. Associate Fellow AIAA.
‡Research Professor.
§Lockheed Martin Professor. Associate Fellow AIAA.
¶Senior Mechanical Engineer. Member AIAA.
**Research Engineer. Member AIAA.

z = spatial coordinate in the Cartesian Z direction, m
δ = condensate film thickness, m
δT = phase change material melting range, K
δT_o = operating temperature range of the vapor chamber thermal energy storage heat sink within phase change material melting range, K
ε = foam porosity
μ_c = dynamic viscosity of condensate, Pa · s
ρ = effective density of phase change material and foam composite, kg/m^3
ρ_c = density of condensate, kg/m^3
ρ_f = density of foam, kg/m^3
ρ_l = density of the liquid phase of phase change material, kg/m^3
ρ_s = density of the solid phase of phase change material, kg/m^3
ρ_v = density of vapor, kg/m^3
ρ_w = density of the thermal energy storage unit column wall, kg/m^3)

I. Introduction

ELECTRONICS in future military systems involve miniaturization, which produces large heat fluxes at the source level. Heat sinks for such systems should be highly efficient and capable of dissipating such large heat fluxes without causing a sharp rise in the system temperature. This paper focuses on the numerical analysis of the heat storage mechanism of a high-performance dual latent heat sink intended for low thermal duty cycle, high heat flux electronic heat sink applications. This heat sink design combines the features of a vapor chamber with rapid thermal energy storage (TES), employing graphite foam inside the heat storage facility along with solid–liquid phase change materials (PCMs). The vapor chamber feature elevates the system thermal conductivity by about 100–1000 times that of pure metallic copper. This feature, coupled with the rapid TES facility in the design, makes this integrated system a useful one for multiple thermal management applications. Because a liquid–vapor phase change is much faster compared with diffusion in a solid–liquid PCM, it is attractive to absorb the pulse heat from the heat source rapidly using a liquid–vapor phase change and then to transfer it to PCM. The use of PCM as a second latent heat sink helps in reducing the size of a condenser that would otherwise consist simply of a metal plate closing the vapor chamber (on the thermally opposite side of the heat source). Complete details of the concept of this dual latent vapor chamber thermal energy storage (VCTES) heat sink can be found in [1]. It is a 7 MJ heat sink (Fig. 1) with a volume of 0.072 m^3 and a weight of 57.5 kg. It is designed to have a low vapor-to-condenser temperature difference (7°C), fast charging ability, environment safe operation, high heat flux capability (500 W/cm^2 over an area of 100 cm^2), and high energy storage density (97 MJ/m^3, 0.122 MJ/kg) over a charging pulse of 140 s. A demonstrative version of the heat sink was designed for the convenience of performing experiments, and this paper focuses on numerically simulating the heat storage phenomenon as applied to this prototype version of the heat sink.

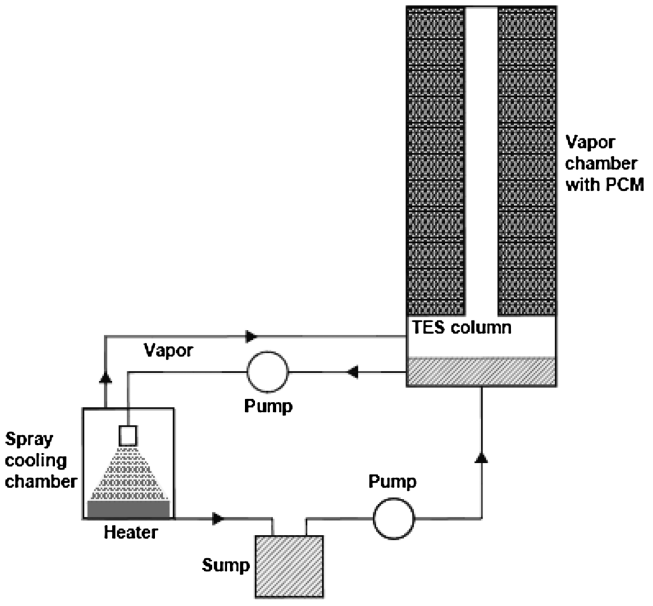

Fig. 1 Schematic of the dual latent VCTES heat sink concept.

The dual latent VCTES sink system thermal operation is characterized by three processes, namely, 1) heat acquisition (by liquid–vapor phase change), 2) heat storage (by vapor flow followed by film condensation on containers with the simultaneous phase change of a PCM inside those containers), and 3) heat rejection (by discharging through the outer surface of the vapor chamber walls).

Of these, the most important process is the heat storage or, more precisely, the swift temporary storage of waste heat using encapsulated phase change materials in a conductive medium. It is because of this rapid temporary thermal energy storage that this heat sink can be designed for an average heat load rather than for pulsed heat loads. But, as most of the available solid–liquid phase change materials have very low thermal conductivities, the heat storage path evolves as the maximum heat resistance path in heat sinks employing PCM for thermal energy storage. But the key feature that enables a fast heat storage mechanism in this heat sink is a coupled or conjugate heat transfer phenomenon wherein the vapor carries heat from the source and condenses on the outside of thermal energy storage containers, while the heat is simultaneously absorbed by phase change materials encapsulated inside those containers in a highly thermally conductive porous graphite foam. Hence, the key focus of this paper is to numerically analyze the key phenomenon of heat storage specific to the aforementioned heat sink.

Most thermal energy storage modeling to date focuses only on the heat absorption process with a constant temperature or constant heat flux condition imposed on the surrounding boundary/encapsulation. This kind of analysis can produce different conclusions compared with the actual situation in the aforementioned integrated dual latent VCTES heat sink, in which the wall boundary condition for the PCM melting comes from the film condensation of vapor on the outer surface of the container walls.

There is no available literature to date that focuses on the conjugate heat transfer problem of transient laminar film condensation coupled with encapsulated PCM melting in porous graphite foams. To the best knowledge of the authors, only limited attention was focused on the numerical analysis of the conjugate transient heat transfer problem of condensation and melting. Contreras and Thorsen [2] were probably the first to analytically study the transient condensation of a saturated vapor on a solid of the same chemical composition coupled with melting of the same solid. They ignored the inertia terms in the momentum equation but included the convective terms in the energy equation and obtained an integral solution using a quadratic temperature profile. Galamba and Dhir [3–5] numerically analyzed the problem of transient condensation of saturated vapor on both normal [3] and subcooled [4] vertical solid walls whose melting temperatures were less than the vapor saturation temperature. The condensing fluid and the melting wall material were assumed immiscible. They used both analytical and numerical techniques for solving the governing equations, which ignored inertia terms in the momentum equation and convective terms in the energy equation. The melt layer physics was treated in a similar way as the condensate film, using analogous parameters for melt layer thickness and steady-state time as for film condensation. This kind of treatment for melting does not hold true if melting occurs in porous media, such as foams, especially in most metal and graphite foams for which the pore size is on the order of a few tens to hundreds of microns. The small pore size in foams will provide a capillary effect and lower the effect of gravity. In addition, it was shown in [6] that there will be practically a minimal temperature difference between the ligaments of a foam and PCM in the pores if the surface area to volume ratio (A/V) for the foam is more than 1575 m^2/m^3. For graphite foams, the A/V is typically on the order of 20,000 m^2/m^3

[7]. These conditions specific to graphite foams will provide a Rayleigh number smaller than the critical value for natural convection in the melt to become significant. Hence, the PCM melting in graphite foams must be modeled as a transient conduction dominated moving melt front problem. Further, the encapsulation of PCM in containers induces wall effects that were not included in any of the previously related works. Chen and Chang [8] studied an analogous conjugate problem of laminar film condensation and natural convection on opposite sides of a vertical wall and included the effect of wall thermal resistance. Char and Lin [9] extended the problem by considering the two media separated by the wall as porous. Both [8,9] were steady-state analyses.

Hence, to numerically solve and understand the transient problem of laminar film condensation coupled with encapsulated solid–liquid PCM phase change inside graphite foam forms an interesting aspect. This would help in better understanding the important parameters that govern the rapidity and efficiency of such temporary heat storage mechanisms in the future as in the current VCTES system.

II. Numerical Model

As mentioned, a fast design tool for this dual latent VCTES system was already developed to facilitate a preliminary design, and this numerical simulation is based on the geometry obtained because of optimizing the design tool for easy and convenient implementation for experiments. Full details of the optimization and theoretical aspects of the design tool can be found in [1]. Individual numerical models for PCM melting inside graphite foam and film condensation on the outside of PCM encapsulating containers are given herein. The coupling of the two models using heat conduction within the TES container walls is also mentioned.

A. Encapsulated Phase Change Material Phase Change in a High Thermally Conductive Porous Graphite Foam

The phase change process of PCM in highly thermally conductive porous graphite foam is solved as a nonlinear transient moving boundary problem. It was observed that the two-temperature model [10] as observed in metal foams can be solved as a one-temperature model [6] in graphite foams owing to the large A/V in graphite foams. The reason for this is explained next.

The actual mode of heat transfer to the PCM in a pore can be assumed as three dimensional through conduction in the foam ligaments. This assumption is equivalent to opening up a cuboid (a hollow rectangular fin) lying in a three-dimensional Cartesian coordinate system into a surface (fin) lying in a two-dimensional coordinate system and assuming that the PCM lies above this fin with a uniform thickness. But when the surface is closed back to form a cuboid, there will be overlapping of PCM volumes. Thus, a two-dimensional model provides for a smaller foam surface area for PCM phase change compared with a cuboid fin model. However, this increase in foam surface area in the cuboid fin model can be alternately captured in the two-dimensional fin model by increasing the number of fins per unit inch. By increasing N above 20, it was shown in [6] that the PCM phase change in porous foams can be modeled using a one-temperature model. This is also true because of a very low heat flux at the pore level when N is a large number. Therefore, it is accurate enough to use a two-dimensional, one-temperature model to model phase change in foams with high N. Whereas $N = 20$ corresponds to a surface area to volume ratio of 1575 m^2/m^3 in [6], POCOFoam®, with a typical surface area to volume ratio of 20,000 m^2/m^3 [7], leads to a value of N much greater than 20. Therefore, a single temperature representative of both the foam and PCM temperatures can be used in the numerical modeling.

Another interesting feature to be noted with respect to heat transfer in graphite foams filled with a PCM is that the heat transfer occurs in series from the column (TES unit) wall to the column center, rather than in a lumped manner in all the foam ligaments first and then in parallel paths in all the pores. This can be better explained by considering an equivalent Biot number as given by Eq. (14) in Lee and Vafai [11]:

$$Bi = \frac{h_{\text{int}} \gamma a W^2}{4k_{\text{fe}}} \tag{1}$$

where $\gamma = 1$ for parallel plate/rectangular configurations [11].

For POCOFoam® enclosed in a container as shown in Fig. 2, $a = 20,000$ [7], $W/2 = 0.0064$ [1], and $k_{fe} = 135$ [12] units. h_{int} can be found from the pore Nusselt number as follows:

$$Nu_p = (h_{\text{int}} d_p / k_{\text{PCM}}) \tag{2}$$

where $d_p = 350\ \mu$m for POCOFoam® [12] and k_{PCM} can be assumed as 0.2 W/m · K (representative of most paraffin waxes). Nu_p can be assumed as 2 [13] by approximating the shape of the PCM interacting with the solid foam as spheres surrounded by POCOFoam®. This gives $h_{\text{int}} = 1143$ W/m^2 · K.

Using the values in Eq. (1), we get $Bi \sim 7$. With $Bi \gg 0.1$, it is clear that the conduction resistance in the foam ligaments is much higher compared with the convective heat transfer resistance at the interface of the foam ligaments and PCM, which implies that the temperature gradient inside the foam ligaments cannot be ignored. Hence, the heat transfer occurs in series from the container wall to the container center portion, rather than in the foam ligaments first followed by parallel paths in all the pores.

As far as the effect of film condensation on the dimensions of the phase change problem is concerned, it must be noted that the column wall temperature will have a variation along the height, and the temperature drop across the film in the cross-stream direction will be about the same or even more compared with the temperature drop in the PCM filling the foam. Therefore, the heat transfer in PCM will be two dimensional.

Based on these conclusions, the model then collapses to solving a phase change problem in the Y–Z plane of the TES column (Fig. 2) by considering the effective thermophysical properties of the

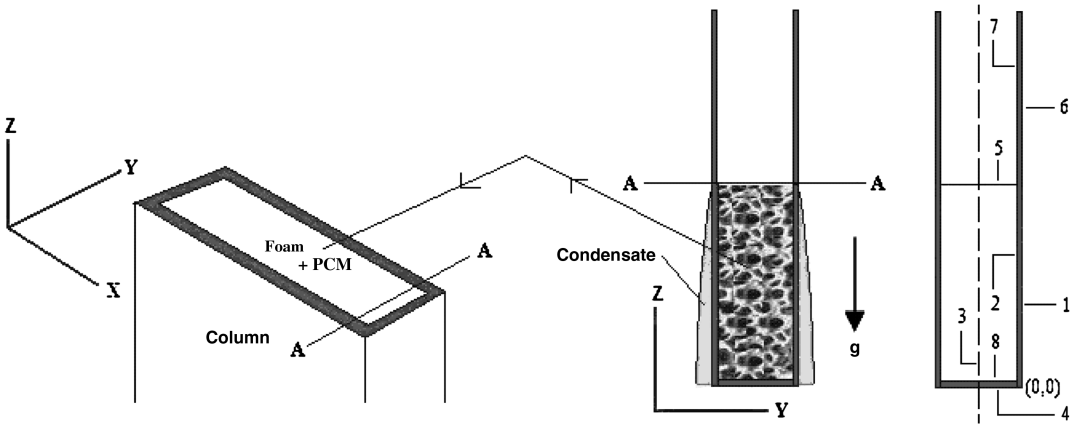

Fig. 2 Schematic of the TES unit considered for numerical simulation.

foam–PCM composite based on the foam porosity. A fixed grid heat capacity formulation [14–16] is used to model this problem. Enthalpy models [17–20] for phase change are attractive in the sense that they do not require explicit tracking of the phase change interface, unlike in the heat capacity methods. But, whereas the heat capacity method provides an explicit temperature field in the phase change domain, the temperature field in an enthalpy model has to be implicitly evaluated using the enthalpy–temperature correlation. In addition, the liquid fraction field is imbibed in the temperature field in the enthalpy models. It has been traditionally observed that, for phase change problems with a melting range and for conjugate heat transfer problems involving adjacent walls, the heat capacity method performs better [16]. Therefore, for the current simulation, an easy-to-implement modified effective heat capacity method is used.

The mathematical model is described below and includes the following assumptions:

1) The effects of natural convection within the molten PCM can be ignored as explained earlier. Therefore, the phase change process is conduction dominated.

2) Temperature gradients in the X direction (Fig. 2) can be ignored owing to the symmetry of the boundary conditions with respect to that direction. This can be justified because the X-direction boundary conditions for the phase change inside the column come from the condensing film on the outside of the column, and the condensate thickness does not vary along the X direction at any time during the TES unit charging process.

3) The thermal conductivity of PCM is different for solid and liquid phases but independent of temperature in any one phase. This assumption is reasonable especially for heavy paraffin waxes (for which the number of carbon atoms is >30) as the one assumed in the current work. Paradela et al. [21] exclusively modeled the thermal conductivities of paraffins used primarily for TES. From Eq. (9) and Table I in [21], it can be seen that the first- and second-order temperature coefficients for most paraffins are very small compared with their zero-order coefficient. In addition, it can be observed that, as the value of number of carbon atoms increases, the first- and second-order temperature coefficients decrease.

4) The density of PCM is different for solid and liquid phases but independent of temperature in any one phase.

5) PCM is homogeneous and isotropic and has no property degradation with time.

6) During refreezing of PCM, voids will be created due to a decrease in PCM volume. These voids will be distributed nonuniformly and create a high thermal resistance path to heat transfer. The initiation and growth of such shrinkage voids was thermodynamically studied in detail by Sulfredge et al. [22]. They found that the number and pattern of nucleation centers available for liquid during solidification is a key factor that determines the void arrangement. Techniques such as promoting artificial nucleation sites were also suggested as possible means of dispersing the voids. Using foam provides such nucleation centers for molten PCM, which makes the voids uniformly distributed and thus enhances the conducting path. As far as void formation near the interface of PCM and foam composite and copper wall is concerned, a good contact between the wall and foam ligaments will mitigate the effect of a small void because heat transfer to the PCM happens by first penetrating from the wall into the foam and then into PCM. If a high thermal conductive epoxy/bond is used to join the copper and foam, it can be assumed that there will be minimum contact resistance at the interface because of void formation. Hence, void formation effects are neglected in the numerical simulation.

For conduction controlled PCM phase change, the transient energy equation in the Cartesian coordinate system in general is given by

$$c_p(T)\frac{\partial T(x,y,z,t)}{\partial t} = \nabla\cdot\left(\frac{k}{\rho}\nabla T(x,y,z,t)\right) \tag{3}$$

Because graphite foams exhibit anisotropic thermal conductivity [7], the numerical model includes the same by defining a two-dimensional tensor for k as follows:

$$[k] = \begin{bmatrix} k_{yy} & 0 \\ 0 & k_{zz} \end{bmatrix} \tag{4}$$

As applied to a column, as shown in Fig. 2, the energy equation then becomes

$$c_p(T)\frac{\partial T(y,z,t)}{\partial t} = \left(k_{yy}\frac{\partial^2 T(y,z,t)}{\partial y^2} + k_{zz}\frac{\partial^2 T(y,z,t)}{\partial z^2}\right)\frac{1}{\rho} \tag{5}$$

Because melting range is a usual characteristic of paraffin waxes, the specific heat is defined as shown in Eq. (6):

$$c_p(T) = \begin{cases} \varepsilon c_{\mathrm{ps}} + (1-\varepsilon)c_{pf}; & T < T_m - (\delta T/2) \\ \varepsilon(c_{pm}) + (1-\varepsilon)c_{pf}; & T_m - (\delta T/2) \le T \le T_m + (\delta T/2) \\ \varepsilon c_{\mathrm{pl}} + (1-\varepsilon)c_{pf}; & T > T_m + (\delta T/2) \end{cases} \tag{6}$$

During melting of PCM, the specific heat is modeled as given in [23]:

$$c_{pm} = h_{sf}/\delta T \tag{7}$$

ρ in Eq. (5) is given by Eqs. (8) and (9), respectively,

$$\rho = \begin{cases} \varepsilon\rho_s + (1-\varepsilon)\rho_f; & T < T_m - (\delta T/2) \\ \varepsilon\left(\frac{\rho_s+\rho_l}{2}\right) + (1-\varepsilon)\rho_f; & T_m - (\delta T/2) \le T \le T_m + (\delta T/2) \\ \varepsilon\rho_l + (1-\varepsilon)\rho_f; & T > T_m + (\delta T/2) \end{cases} \tag{8}$$

$$k_{yy} = \begin{cases} \varepsilon k_s + (1-\varepsilon)k_{fy}; & T < T_m - (\delta T/2) \\ \varepsilon\left(\frac{k_s+k_l}{2}\right) + (1-\varepsilon)k_{fy}; & T_m - (\delta T/2) \le T \le T_m + (\delta T/2) \\ \varepsilon k_l + (1-\varepsilon)k_{fy}; & T > T_m + (\delta T/2) \end{cases} \tag{9}$$

k_{zz} is defined similarly as in Eq. (9).

Initial Condition:

$$T(y,z,0) = T_0 \tag{10}$$

Boundary Conditions:

1) $\mathbf{q}\cdot\hat{n} = 0$ on boundary 3.

2) Temperature and heat flux continuity on boundaries 2 and 8.

3) $\mathbf{q}\cdot\hat{n} = h[T(y, L + t_w, t) - T_{\mathrm{inf}}]$ on boundary 5.

B. Laminar Film Condensation on a Flat Vertical Surface

An analysis of laminar transient film condensation on a vertical plate was done by Sparrow and Siegel [24], Reed et al. [25], and Chung [26]. It was shown in [24,25] that the transient problem can be treated as quasi steady provided Ja and Ja/Pr are both $\ll 1$. This implies that the temperature profile is linear and the velocity profile is parabolic.

It must be noted that, in [25], it was shown that the aforementioned condition on Ja and Ja/Pr holds true for water in atmospheric conditions, whereas the actual conditions in the dual latent VCTES heat sink are usually not atmospheric [1]. In addition, Ja depends on the temperature difference across the liquid film, which differs from case to case. Hence, appropriate values for thermophysical properties of water for conditions in the vapor chamber (P_{sat} of approximately 2 atm) were used to evaluate Ja and Pr for application to the current problem under consideration. Because the film thickness will be small, the temperature difference across the film will be small ($\sim$1 K). It was found that $Ja = 0.0019$ and $Ja/Pr = 0.0014$. Even for a temperature difference across the film of 10 K (which is highly unlikely), Ja and Pr are 0.019 and 0.014, respectively, with both much smaller than unity. Therefore, a quasi-steady approach can be used.

The film thickness in any given time step can be reasonably approximated using the boundary conditions as shown in Eq. (12), in which the variation in the wall temperature in the column height direction is also included:

$$\delta(z,t) = \left[\frac{4k_c\mu_c \int_0^L (T_v - T_{\text{wall}}(z,t))\,\mathrm{d}z}{h_{lv}g(\rho_c - \rho_v)\rho_c}\right]^{0.25} \tag{12}$$

C. Heat Conduction in the Solid Wall Encapsulating the Phase Change Material

A two-dimensional energy equation in Cartesian coordinates was solved in the solid wall as shown in Eq. (12).

$$c_{pw}\frac{\partial T_w(y,z,t)}{\partial t} = \left(\frac{\partial^2 T_w(y,z,t)}{\partial y^2} + \frac{\partial^2 T_w(y,z,t)}{\partial z^2}\right)\frac{k_w}{\rho_w} \tag{13}$$

Initial Condition:

$$T_w(y,z,0) = T_0 \tag{14}$$

Boundary Conditions:

4) $\mathbf{q}\cdot\hat{n} = 0$ on boundary 4.

5) $T(0,z,t) = T_{\text{wall}}(z,t)$ on boundary 1.

D. Numerical Coupling

In the numerical problem, coupling is required at two junctions: between condensing film and the column outer wall (boundary 1 in Fig. 2), and between the column inner wall (boundary 2 in Fig. 2) and the composite region of graphite foam and PCM. Coupling is done using the temperature and heat flux continuity at both the interfaces.

The assumptions made for the numerical coupling are as follows:

1) The vapor temperature T_v is a constant. This was assumed because the goal of this work is to approximately model and qualitatively study the use of having a heat storage mechanism in the system but not to simulate the complexities involved in the overall system combining the two latent phase change processes.

2) The heat transfer coefficients for heat removal on the column boundaries 6 and 7 (Fig. 2) were chosen to be 50 and 5 $\text{W/m}^2\,\text{K}$ for the column outside and inside faces, respectively, assuming the modes of heat removal from those faces as forced and natural convection, respectively [13]. This is reasonable because forced convection can only be used on the outside surfaces of columns and not on the inside surfaces, as shown in Fig. 2.

The following solution procedure is implemented:

1) Solve the PCM and graphite foam composite phase change problem.

2) Solve for $\delta(z,t)$.

3) Get $T_{\text{wall}}(z,t)$ using the temperature and heat flux continuity at the column wall and condensate interface.

4) Go to the next time step.

5) Repeat steps 1–4 until the end of the charging period.

The finite element method is used to solve the system of equations. A commercial finite element code, COMSOL® [27], along with MATLAB® [28], is used, and user-defined modules for solving PCM phase change in graphite foam and condensate film thickness are incorporated.

III. Results and Discussion

Because no experiments have been performed to check the validity of the current PCM phase change model, it is first verified with one of the experimental results described in [29], wherein a cylindrical copper block was attached to a cylindrical piece of Poco Graphite foam. The copper block was made to act as a heat source by using an external heater attached to its top surface. The entire assembly was then immersed into a Teflon enclosure serving as thermal insulation. The graphite foam was a priori filled with paraffin wax. A schematic of the setup is shown in Fig. 3. Experiments were performed for different heat inputs, and the transient temperature distribution of the PCM at locations 2, 3, and 4 of the foam and PCM composite are plotted in Fig. 8 in [29]. A case in which the heat input was 11.63 W is selected to validate the current model. The same setup and boundary conditions are implemented, and thermocouple locations 2, 3, and 4 are picked to be at exactly the same locations as described in [29] and bear the same numbering. For a better comparison, the results are overlapped onto Fig. 8 in [29] and are shown in Fig. 4. It can be observed that the results of the current model with assumptions mostly overlapped those in Fig. 8 in [29] and so can reasonably simulate PCM phase change in graphite foams. Because, in [29], individual details of the thermophysical properties of PCM, foam, and the heat transfer coefficient for natural convection were not mentioned, typical values for those mentioned in the literature were taken (5 $\text{W/m}^2\,\text{K}$ for the heat transfer coefficient [13]).

After verification, the phase change model is used to analyze the effectiveness of the heat storage phenomenon in the demonstrative version with the corresponding TES column dimensions ($L \sim 0.023$ m, $W \sim 0.01$ m, and $t_w \sim 0.00163$ m), material (copper), and thermocouple nomenclature.

The PCM is assumed to be POLYWAX® 1000, and the differential scanning calorimetry (DSC) curve for the PCM is shown in Fig. 5. The following thermophysical properties are used in the numerical simulation: $c_{ps} = 2900\ \text{J/kg}\cdot\text{K}$, $c_{pl} = 3500\ \text{J/kg}\cdot\text{K}$, $h_{sf} = 266\ \text{kJ/kg}$, $\rho_s = 970\ \text{kg/m}^3$, and $\rho_l = 900\ \text{kg/m}^3$. Because thermal conductivities of the solid and liquid phases of the wax are not known/measured, the typical values of thermal conductivities ($k_s = 0.20\ \text{W/m}\cdot\text{K}$, $k_l = 0.18\ \text{W/m}\cdot\text{K}$) available in the literature for most paraffin waxes are used. Corresponding values for graphite foam are taken as $c_{pf} = 1730\ \text{J/kg}\cdot\text{K}$, $\rho_f = 2200\ \text{J/kg}\cdot\text{K}$, $k_{fy} = 135\ \text{W/m}\cdot\text{K}$ (out of plane), and $k_{fz} = 45\ \text{W/m}\cdot\text{K}$ (in-plane). The porosity for graphite foam is taken as 0.75 [7].

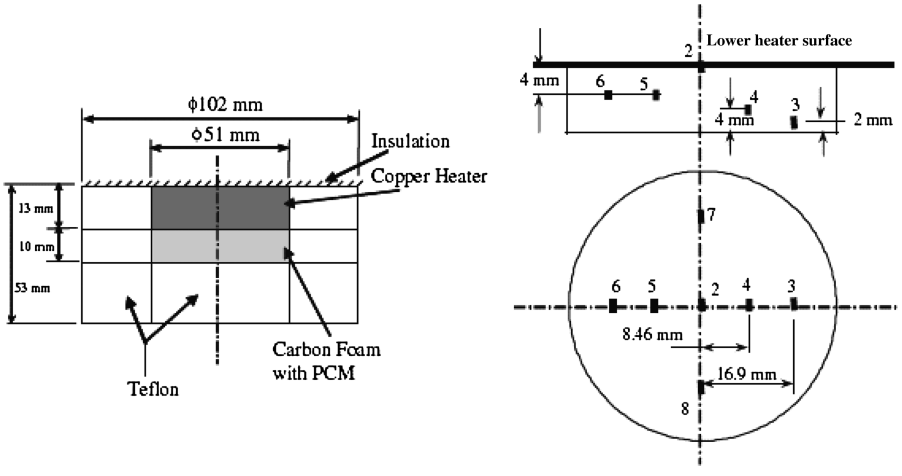

Fig. 3 Schematic of the thermal protection cell as given in [29] with thermocouple locations.

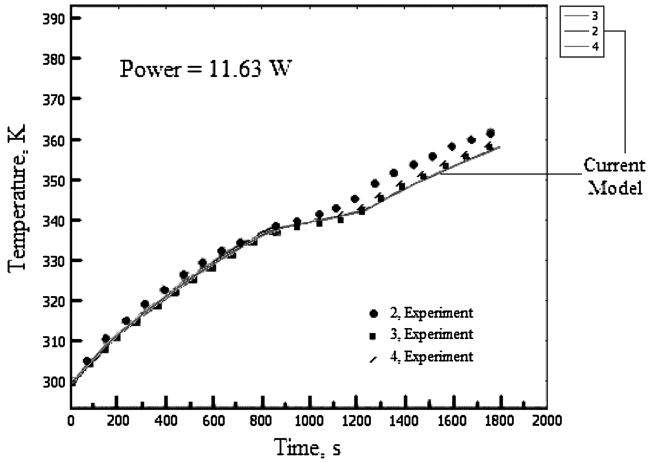

Fig. 4 Comparison of the current model with the experimental results of [29].

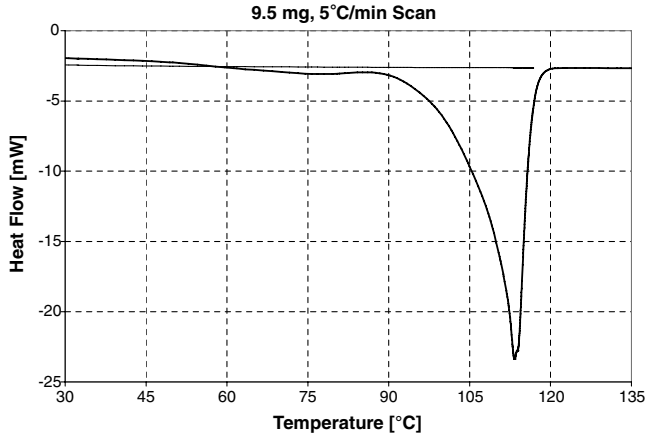

Fig. 5 DSC curve of PCM.

The chosen PCM has a wide range of melting and so, to use the latent heat of PCM effectively by simultaneously not sacrificing the narrow temperature operation of the device, an operating temperature range within the melting range of PCM is chosen for which the latent heat is a maximum. This is achieved by integrating the DSC curve over a chosen operating range to obtain the area and, hence, the heat of fusion for that range of temperature. For example, if an operating range of 8 K is chosen, then there will be multiple options within the melting range (363–393 K), but only one of them corresponds to a maximum heat of fusion. The best ranges of operation for all the possibilities within the melting range are found, and an operating range of 8 K from 380 to 388 K is chosen, for which the latent heat is, $h_{sfo} = 138$ kJ/kg.

Based on this, c_{pm} is redefined for this particular simulation as

$$c_{pm} = h_{sfo}/\delta T_o \tag{16}$$

The default unstructured meshing option available in the software program was used to mesh the geometry. This avoided the matching constraints on the node number on different length boundaries that needed to be taken care of during manual structured meshing. Three unstructured meshes consisting of 13,404, 53,616, and 214,464 triangular elements were used to perform a grid independency check on the final solution. The minimum mesh element quality was 0.62, and the average mesh quality was more than 0.8 for all three meshes. It was found that the final solution, on average, improved by less than 0.15 K as the mesh was refined to contain more than 13,404 elements. Therefore, the same mesh was used for all the simulations. In addition, for all the simulations, a relative tolerance of $1e-4$ was used to check for the convergence of the solution in any single time step.

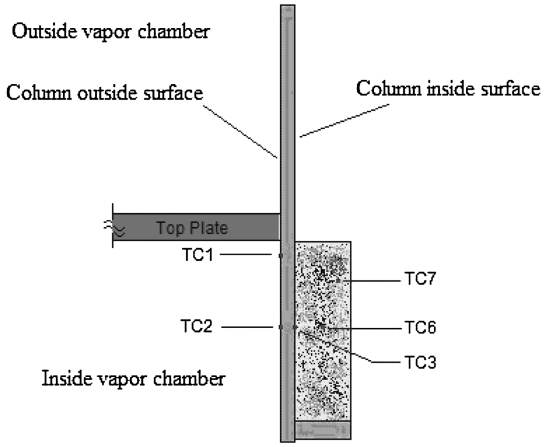

Fig. 6 Temperature measurement locations in the numerical model.

TC3, TC6, and TC7 in Fig. 6 are the temperature measurement locations in the foam and PCM composite. Two more locations, TC1 and TC2, were chosen for the numerical simulation to monitor the outside wall temperature of the TES column. In Fig. 6, TC7 is located at 6 mm and TC2, TC3, and TC6 are located at 12 mm, all in the vertical direction from the top surface of the foam (boundary 5 in Fig. 2). TC1 is chosen to be any point very close to the foam top surface. In the horizontal direction, TC1 and TC2 lie on the column wall outside, whereas TC3 lies on boundary 2 in Fig. 2. TC6 lies at a distance of $W/4$ and TC7 lies at a distance of $3W/8$, both from the column inside wall.

A T_v of 390 K, a T_0 of 380 K, and a charging time of 15.5 s are chosen for all the simulations. Figure 7 shows the simulated time history of the temperature at the various thermocouple locations in Fig. 6.

The following observations and conclusions can be drawn from Fig. 7:

1) The wall temperature drops rapidly from an initial value of chosen vapor temperature because of the presence of a heat sink (PCM) and then begins to rise slowly.

2) The dominant resistance during charging is from the condensate film. Once a steady state is reached (a long time after the end of charging), the film and PCM resistances become comparable [1].

3) The presence of a varying thickness condensate film makes the PCM phase change problem two dimensional, as expected.

4) The PCM temperature governs all other parameters, such as T_{wall} and δ.

5) Heat penetration into PCM is mostly from the top portion of the column wall, where the film thickness is small because of a small thermal penetration resistance. This can be verified by comparing TC7 with TC6.

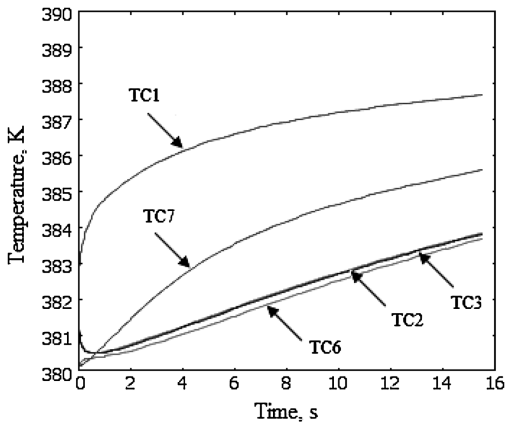

Fig. 7 Temperature vs time for PCM with a melting range.

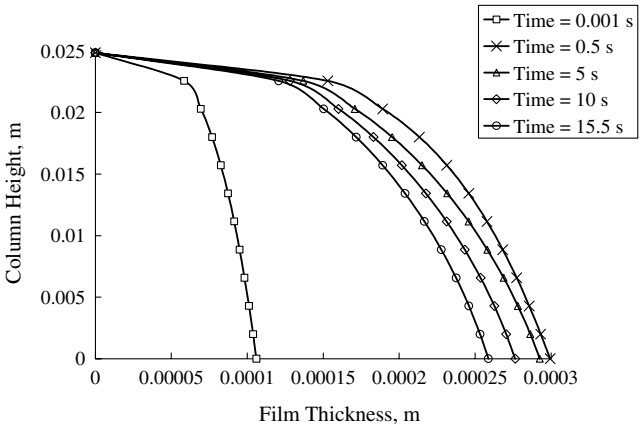

Fig. 8 Transient film profile history (film thickness at time = 0 s is zero).

6) The initial temperature choice T_0 of the PCM is appropriate because, on an average, the PCM temperature rose from 380 (107) to 384.5 K (111.5°C), a range in which the latent heat h_{sfo} is a maximum within the PCM's entire melting range as discussed earlier.

7) That the PCM temperature at the end of the charging time is still less than T_v implies that the vapor temperature will not rise before the end of the charging period. This means that PCM is helpful in preventing the undue rise of temperature and pressure inside the vapor chamber.

Figure 8 shows the time evolution of the condensate film during the charging time. The variable "time" spans from 0 to 15.5 s and is the same in both the figures. In Fig. 8, it can be observed that the average film thickness at time = 0 s is zero, whereas, at time = 0.001 s, it is about 81 μm, and, at time = 0.5 s, δ increases on average to 226 μm. This corresponds to the initial rapid cooling of the wall from T_v at time = 0 s to a much lower value at time = 0.5 s, as can be seen in Fig. 7. As T_{wall} starts to rise again, the film thickness starts going down until the end of the charging time to an average value of 190 μm.

Using Fig. 7, it is found that 81% of the total absorbed heat is by the PCM and foam composite, whereas the remaining 19% is by the encapsulating column walls. This shows the importance of including the column wall inertia effects in the simulation of the conjugate problem for the chosen boundary conditions. In addition, the inclusion of column walls in the model facilitates the simulation of simultaneous heat removal on the extended portion of the columns, that is, boundaries 6 and 7 in Fig. 2 that protrude outside the vapor chamber, as shown in Fig. 6.

A. Importance of Having Thermal Energy Storage in the Vapor Chamber Thermal Energy Storage Heat Sink

The effect of the presence of PCM on the charging of the VCTES heat sink can be observed in Fig. 9, in which the PCM was replaced with air for comparison with Fig. 7. It can be seen that the wall temperature drops down initially. However, because the sink in this case is not as effective as in Fig. 7, the wall temperature starts to rise rapidly and catches up with the vapor temperature even before the end of the charging time.

If the vapor temperature was not fixed, as in the current model, this will cause a continuous increase in the vapor temperature and, hence, the pressure inside the chamber. It can also be observed by comparing Figs. 7 and 9 that, in Fig. 9, the temperature rise is purely characteristic of transient heat conduction as in a solid but, in Fig. 7, the temperature rise is in a more linear fashion because of PCM phase change.

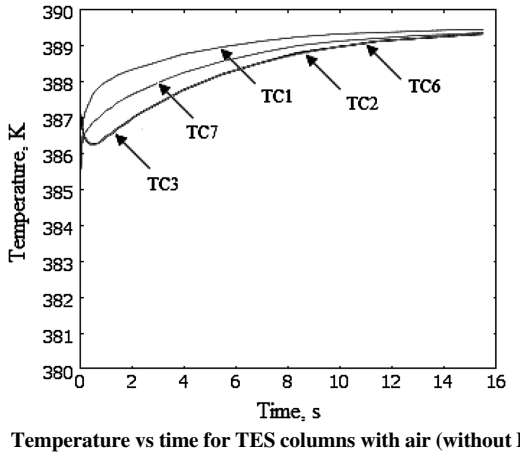

Fig. 9 Temperature vs time for TES columns with air (without PCM).

B. Importance of Phase Change Material

In Fig. 10, the effect of using a pure PCM is analyzed and plotted. Pure PCMs are characterized by isothermal melting (here, 386 K); hence, the effect of full latent heat can be felt on the heat sink system. PCMs, such as the one used to simulate the case of Fig. 7, will have a reduction in the latent heat peak owing to the distribution of latent heat over a melting range (shown in Fig. 5). The effect of melting range on the TES performance was studied and mentioned in [1]. Heat capacity methods exhibit problems in simulating ideal isothermal melting and so usually enthalpy methods are used. Therefore, a δT of 0.001 K is used to approximately model the phase change process for this case and the entire h_{sf} of 266 kJ/kg is assumed to be distributed over this δT. Three more cases for a δT of 0.01, 0.0001, and 0.00001 K were run. It was found that the time taken to reach a converged solution at each time step almost doubled as δT became smaller. A difference of less than 0.01 K on average was found between final solutions for δT of 0.001 and 0.0001 K, and this difference became less than 0.005 K as δT went down. Therefore, a δT of 0.001 K was selected for the simulation, as achieving an accuracy of the final solution of more than two significant digits is not the goal of this simulation but rather it is to broadly see the effect of using pure PCM. The temperature–time history of PCM in Fig. 10 is typical of pure PCMs. An initial cooling down of the wall temperature can be observed because of the presence of an effective heat sink (just like in Fig. 7). The wall temperature begins to rise again but remains almost constant when the PCM reaches its melting point and continues to stay there even until the end of charging time.

The same initial temperature as chosen in the simulation of Fig. 7 was used also in the simulation of Fig. 10 and so we could observe the rapid initial temperature rise in the beginning (the period of no PCM phase change). The advantage of pure PCMs can be very clearly seen if an initial temperature is chosen that is slightly less than the PCM melting temperature. For example, in the case of Fig. 10, if an initial temperature of 385.9 K was chosen, the entire operating temperature of PCM during charging period would have remained at 386 K and the wall temperature would have remained almost the same between 386.5 and 387.5 K. In Fig. 7, because the PCM has a melting range, it

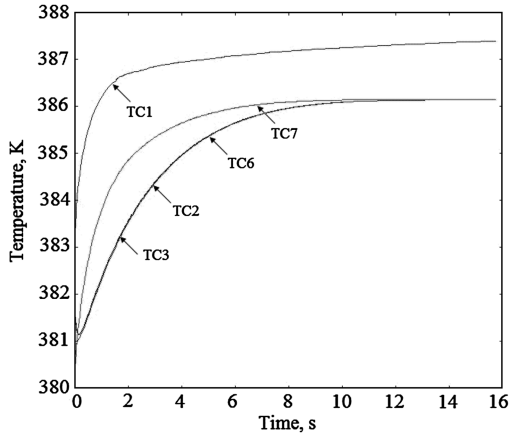

Fig. 10 Temperature vs time for pure PCM (with near-isothermal melting point).

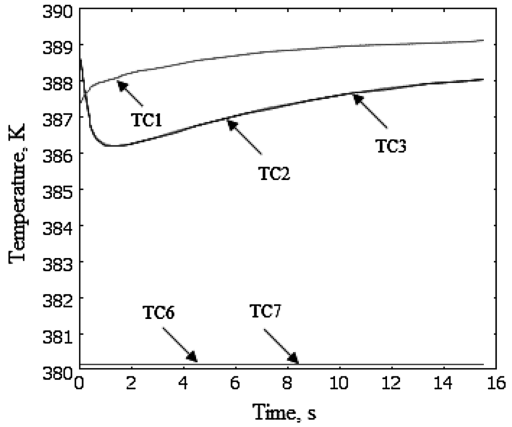

Fig. 11 Temperature vs time for TES columns without graphite foam.

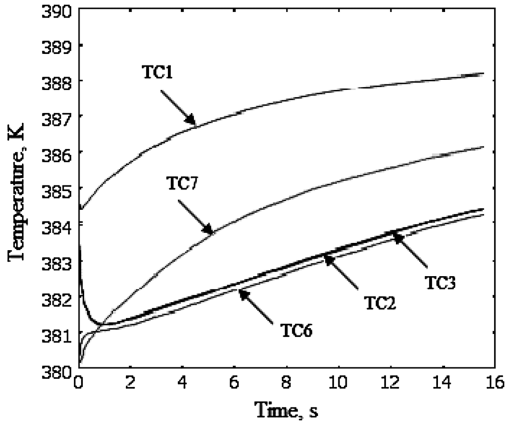

Fig. 12 Temperature vs time for TES columns with natural convection heat removal to air.

is inevitable to pick an initial temperature much less than the melting point peak to allow for the PCM temperature rise during melting.

Thus, it is evident that pure PCMs provide better performance and near-isothermal operation of the VCTES heat sink. It is interesting to note that the developed numerical model has few convergence problems even in solving an isothermal phase change problem, which is highly nonlinear compared with phase change problems with a melting range.

C. Importance of Graphite Foam in Thermal Energy Storage

The developed numerical model was also used to study the importance of using foam in TES units. Accordingly, only PCM was assumed present in the columns without any thermal conduction-enhancing medium (graphite foam). The results are shown in Fig. 11. The wall temperature drops initially because of the presence of a sink in the form of copper walls and PCM, but this drop is not quite as much as in Fig. 7. This is because, in Fig. 11, the majority of the heat sink is composed only of copper walls because of the poor penetration of heat in the PCM sans graphite foam. This could be clearly observed in Fig. 11, in which TC6 and TC7 are still at the initial temperature at the end of the charging time indicating, that no melting of PCM has taken place at those locations. Therefore, owing to its poor thermal conductivity, the resistance to heat transfer in PCM without graphite foam dominates the film condensation resistance during the transient charging process.

D. Importance of Heat Removal Mechanism to Air on the Performance

In the assumptions for the numerical simulation, it was assumed that heat removal to air from the outside surfaces of the TES columns in Fig. 2 is by forced convection. To see the effect of the heat rejection mechanism to air on the performance of the storage feature in the heat sink, natural convection was assumed even on the outside surfaces of the TES columns, and the results for this case are shown in Fig. 12. It can be observed that the system temperature is, on average, greater by about 0.5 K for this case compared with Fig. 7, as expected. This shows that an efficient heat removal mechanism to air can lower the system temperature rise for fixed charging period conditions.

IV. Conclusions

A numerical analysis of the heat storage mechanism in a dual latent heat sink intended for low thermal duty cycle electronic heat sink applications is presented in this paper. The key process of heat storage during the pulse heat generation period of the duty cycle for this heat sink is composed of the transient simultaneous laminar film condensation of vapor and the melting of an encapsulated phase change material in graphite foam. The problem is numerically analyzed including the wall inertia effects. An effective heat capacity formulation is employed for modeling the phase change problem and is solved using the finite element method. The developed model is useful in qualitatively analyzing the considered conjugate problem in future similar applications and provides a simple way to investigate the usefulness of certain key features of the heat storage units of the heat sink, which otherwise consume too much experimental time.

The results of the developed model showed that the concept is effective in preventing an undue temperature rise of the heat source. The advantage of having a second latent phase change phenomenon in the heat sink in the form of PCM phase change is shown by assuming the lack of PCM in the design. It is also numerically shown that pure PCM exhibits a better performance. The significance of having a thermal conductivity enhancing medium for PCM is also shown. As expected, graphite foam plays a very crucial role in transferring heat to the PCM and thus helps in rapid charging.

It is found that, during the transient operation of a dual latent VCTES heat sink, the key impediment to rapid heat absorption comes from the condensate film. Because of the condensate profile, the PCM phase change problem becomes two dimensional and the temperature gradient in the interfacial solid wall in the height direction is large. It is also observed that, for PCMs with a melting range, the selection of a correct operating range and initial temperature is crucial.

Acknowledgment

The authors sincerely wish to thank Michele Puterbaugh, the program manager at Universal Technology Corporation, Dayton, Ohio, for funding the work.

References

[1] Kota, K., Chow, L., Du, J., Kapat, J., Leland, Q., and Harris, R., "Design of a Dual Latent Heat Sink for Pulsed Electronic Systems," *Journal of Thermophysics and Heat Transfer*, Vol. 22, No. 4, 2008, pp. 572–580. doi:10.2514/1.34998

[2] Contreras, W., and Thorsen, R. S., "Transient Melting of a Solid Heated by a Condensing Saturated Vapor—Case 1: Negligible Interface Curvature," *Journal of Heat Transfer*, Vol. 97, Nov. 1975, pp. 570–575.

[3] Galamba, D., "Some Aspects of Simultaneous Melting—Condensation on Vertical Surfaces," Ph.D. Dissertation, Department of Mechanical and Aerospace Engineering, University of California, Los Angeles, 1985.

[4] Galamba, D., and Dhir, V. K., "Transient Simultaneous Condensation and Melting of a Vertical Surface," *Journal of Heat Transfer*, Vol. 107, No. 4, 1985, pp. 812–818.

[5] Galamba, D., and Dhir, V. K., "Transient Condensation—Melting of a Subcooled Vertical Surface," *Numerical Heat Transfer*, Vol. 15, Feb. 1989, pp. 33–65. doi:10.1080/10407788908944676

[6] Du, J., Chow, L., and Leland, Q., "Optimization of High Heat Flux Thermal Energy Storage with Phase Change Materials," American Society of Mechanical Engineers Paper IMECE2005-80327, 2005.

[7] Klett, J., "High Thermal Conductivity, Mesophase Pitch-Derived Graphitic Foams," *Journal of Composites in Manufacturing*, Vol. 15, No. 4, 1999, pp. 1–7.

[8] Chen, H., and Chang, S., "Coupling Between Laminar Film Condensation and Natural Convection on Opposite Sides of a Vertical

Plate," *International Journal for Numerical Methods in Fluids*, Vol. 24, 1997, pp. 319–336.
doi:10.1002/(SICI)1097-0363(19970215)24:3<319::AID-FLD496>3.0.CO;2-E

[9] Char, M., and Lin, J., "Conjugate Film Condensation and Natural Convection Between Two Porous Media Separated by a Vertical Plate," *Acta Mechanica*, Vol. 148, 2001, pp. 1–15.
doi:10.1007/BF01183665

[10] Krishnan, S., Murthy, J., and Garimella, S., "A Two-Temperature Model for the Analysis of Passive Thermal Control Systems," *Journal of Heat Transfer*, Vol. 126, 2004, pp. 628–637.
doi:10.1115/1.1773194

[11] Lee, D., and Vafai, K., "Analytical Characterization and Conceptual Assessment of Solid and Fluid Temperature Differentials in Porous Media," *International Journal of Heat and Mass Transfer*, Vol. 42, 1999, pp. 423–435.
doi:10.1016/S0017-9310(98)00185-9

[12] Wiechmann, L., "Graphite Foam with High Thermal Conductivity and Diffusivity Conducts Heat in All Directions," *Materials Research Society Bulletin*, Vol. 25, No. 12, 2000, pp. 10–11.

[13] Incropera, F. P., DeWitt, D. P., Bergman, T. L., and Lavine, A. S., *Fundamentals of Heat and Mass Transfer*, 6th ed., Wiley, New York, 2007.

[14] Morgan, K., "A Numerical Analysis of Freezing and Melting With Convection," *Computer Methods in Applied Mechanics and Engineering*, Vol. 28, No. 3, 1981, pp. 275–284.
doi:10.1016/0045-7825(81)90002-5

[15] Hsiao, J. S., and Chung, B. T. F., "An Efficient Algorithm for Finite Element Solution to Two-Dimensional Heat Transfer with Melting and Freezing," *Journal of Heat Transfer*, Vol. 108, No. 2, 1986, pp. 462–464.

[16] Cao, Y., and Faghri, A., "A Numerical Analysis of Phase-Change Problems Including Natural Convection," *Journal of Heat Transfer*, Vol. 112, No. 3, 1990, pp. 812–816.
doi:10.1115/1.2910466

[17] Voller, V. R., and Cross, M., "Accurate Solutions of Moving Boundary Problems Using the Enthalpy Method," *International Journal of Heat and Mass Transfer*, Vol. 24, 1981, pp. 545–556.
doi:10.1016/0017-9310(81)90062-4

[18] Voller, V. R., "Implicit Finite Difference Solutions of the Enthalpy Formulation of Stefan Problems," *IMA Journal of Numerical Analysis*, Vol. 5, 1985, pp. 201–214.
doi:10.1093/imanum/5.2.201

[19] Voller, V. R., Cross, M., and Markatos, N. C., "An Enthalpy Method for Convection/Diffusion Phase Change," *International Journal for Numerical Methods in Engineering*, Vol. 24, 1987, pp. 271–284.
doi:10.1002/nme.1620240119

[20] Voller, V. R., "Fast Implicit Finite Difference Method for the Analysis of Phase Change Problems," *Numerical Heat Transfer, Part B, Fundamentals*, Vol. 17, 1990, pp. 155–169.
doi:10.1080/10407799008961737

[21] Paradela, F., Queimada, A., Marrucho, I., Neto, C., and Coutinho, J., "Modeling the Thermal Conductivity of Pure and Mixed Heavy *n*-Alkanes Suitable for the Design of Phase Change Materials," *International Journal of Thermophysics*, Vol. 26, No. 5, Sept. 2005, pp. 1461–1475.
doi:10.1007/s10765-005-8097-2

[22] Sulfredge, D. C., Chow, L. C., and Tagavi, K. A., "Initiation and Growth of Solidification Shrinkage Voids," *Annual Review of Heat Transfer*, Vol. 10, edited by C.-L. Tien, Begell House, Inc.,1999.

[23] Bart, G. C. J., and van der Laag, P. C., "Modeling of Arbitrary-Shaped Specific and Latent Heat Curves in Phase Change Storage Simulation Routines," *Journal of Solar Energy Engineering*, Vol. 112, 1990, pp. 29–33.
doi:10.1115/1.2930755

[24] Sparrow, E. M., and Siegel, R., "Transient Film Condensation," *Journal of Applied Mechanics*, Vol. 26, March 1959, pp. 120–121.

[25] Reed, J. G., Gerner, F. M., and Tien, C. L., "Transient Laminar-Film Condensation on a Vertical Plate," *Journal of Thermophysics and Heat Transfer*, Vol. 2, No. 3, 1988, pp. 257–263.
doi:10.2514/3.94

[26] Chung, P. M., "Unsteady Laminar Film Condensation on Vertical Plate," *Journal of Heat Transfer*, Vol. 85, Feb. 1963, pp. 63–70.

[27] COMSOL Multiphysics, Modeling Package, Ver. 3.3, COMSOL, Inc., Burlington, MA, 1997–2007.

[28] MATLAB—The Language of Technical Computing, The Mathworks, Inc., Natick, MA, 1994–2007.

[29] Mesalhy, O., Lafdi, K., and Elgafy, A., "Carbon Foam Matrices Saturated with PCM for Thermal Protection Purposes," *Carbon*, Vol. 44, 2006, pp. 2080–2088.
doi:10.1016/j.carbon.2005.12.019